

Superlattice Quantum Critical Point in the Cubic Metal (Sr/Ca)₃Ir₄Sn₁₃

Lina E. Klintberg,¹ Swee K. Goh,^{1,*} Patricia L. Alireza,¹ Paul J. Saines,² David A. Tompsett,^{1,†} Peter W. Logg,¹ Jinhu Yang,^{3,4} Bin Chen,^{3,4} Kazuyoshi Yoshimura,⁴ and F. Malte Grosche¹

¹*Cavendish Laboratory, University of Cambridge,
J.J. Thomson Avenue, Cambridge CB3 0HE, United Kingdom*

²*Department of Materials Science and Metallurgy, University of Cambridge,
Pembroke Street, Cambridge CB2 3QZ, United Kingdom*

³*Department of Physics, Graduate School of Science,
Hangzhou Normal University, Hangzhou 310036, China*

⁴*Department of Chemistry, Graduate School of Science, Kyoto University, Kyoto 606-8502, Japan*
(Dated: February 15, 2012)

Using single crystal x-ray diffraction we show that the quasi-skutterudite system (Sr/Ca)₃Ir₄Sn₁₃ undergoes a temperature driven structural transition at T^* from a simple cubic phase, the I -phase, to the superlattice variant, the I' -phase, which has a lattice parameter twice that of the high temperature phase. We demonstrate that the superlattice transition temperature T^* can be suppressed to zero by both chemical and physical pressure, enabling the first comprehensive investigation of a superlattice quantum critical point and its interplay with superconductivity in a three-dimensional charge density wave system.

Structural self-organisation is a central theme in condensed matter physics. Often, the symmetry of a given parent structure is lowered by subtle structural variations which decrease the electronic degeneracy and thereby the total energy. Examples include Jahn-Teller [1] and Peierls distortions [2] and, more generally, modulated lattice distortions, or superlattices. A very diverse family of materials can be explored within the general $R_3T_4X_{13}$, or 3-4-13, stoichiometry, where R is an earth alkaline/rare-earth element, T is a transition metal and X is a group-IV element. Among these are the superconducting and magnetic stannides [3, 4] for which this structure was first reported, Ce-based Kondo lattice systems [5], and thermoelectrics [6]. Many members of this family adopt variant structures derived from the simple cubic parent structure (I -phase, $Pm\bar{3}n$). Empirically, compounds with divalent or tetravalent cations R occur in the I -phase, whereas compounds with trivalent cations form in the I' -phase. Detailed diffraction studies [7–9] disagree about the precise I' -phase structure, but consistently interpret the distortion as a deformation of the X_{12} cages, which can be viewed as a weak superlattice formation of the I -phase with twice the lattice constant.

A recent reexamination of superconducting Ca₃Ir₄Sn₁₃ [10] revealed distinct anomalies in the electrical resistivity and magnetic susceptibility at $T^* \simeq 33$ K. In the isoelectronic sister-compound Sr₃Ir₄Sn₁₃ the equivalent anomaly occurs at $T^* \simeq 147$ K. Intermediate compositions (Ca_{*x*}Sr_{1-*x*})₃Ir₄Sn₁₃ form readily; this invites studies exploiting the negative chemical pressure from partial substitution of Ca by Sr, together with positive physical pressure from a hydrostatic pressure cell. In this Letter, we report a detailed investigation of the nature of the transition at T^* by x-ray diffraction (XRD), and we examine the dependence of T^* and of the superconducting and normal state properties on physical and chemical pressure. We find that (i) the T^* anomaly is produced by a second order superlattice transition into the I' -phase at low temperature, (ii) T^* is suppressed with increasing pressure and extrapolates to zero temperature near

$p_c \simeq 18$ kbar in Ca₃Ir₄Sn₁₃, giving rise to a structural quantum critical point and (iii) T_c peaks near p_c and the electrical resistivity adopts a linear temperature dependence over a wide temperature and magnetic field range near this critical pressure.

The (Ca_{*x*}Sr_{1-*x*})₃Ir₄Sn₁₃ single crystals were grown by a flux method [4]. Four-wire resistivity measurements were performed using a piston-cylinder cell and a Quantum Design physical property measurement system (PPMS-9). Two Moissanite anvil cells were prepared for AC susceptibility measurements with a conventional mutual inductance method, in which a 10-turn micro-coil [11–13] is placed inside the gasket hole (thickness: 150 μm , diameter: 400 μm) as the pickup coil. Glycerin was used as the pressure medium for the piston-cylinder cell and for one of the anvil cells, and 4:1 methanol-ethanol mixture was used for the other anvil cell. Ruby fluorescence spectroscopy and the superconducting transition of lead were used to determine the pressure in the anvil and piston-cylinder cell respectively. Single crystal XRD measurements were performed using an Oxford Diffraction Gemini E Ultra utilising MoK α radiation at 100 to 295 K, and the structures were solved using direct methods and refined using Shelx-97 [14] via the WinGX interface [15]. The electronic structure was calculated using the the Generalized Gradient Approximation [16] with Wien2k [17]. The experimental lattice parameters of $a = 9.7437$ Å [10] and $a = 9.8100$ Å at 295 K was employed for Ca- and Sr₃Ir₄Sn₁₃, respectively. $Rk_{max} = 7$ and 40,000 k -points were used in a non-spin polarized calculation. The position of the 24k Sn site (0, y , z), the only free internal coordinate, was optimised numerically, resulting in (0, $y = 0.3045$, $z = 0.1516$) and (0, $y = 0.3027$, $z = 0.1522$) for Ca- and Sr₃Ir₄Sn₁₃ respectively.

Room temperature single crystal XRD on Sr₃Ir₄Sn₁₃ confirms the I -phase structure ($Pm\bar{3}n$). However, below T^* the XRD data show additional superlattice reflections which are inconsistent with the I -phase. They must instead be indexed to the I' -phase, a body(I)-centered cubic structure ($I\bar{4}3d$) with a lattice parameter twice that

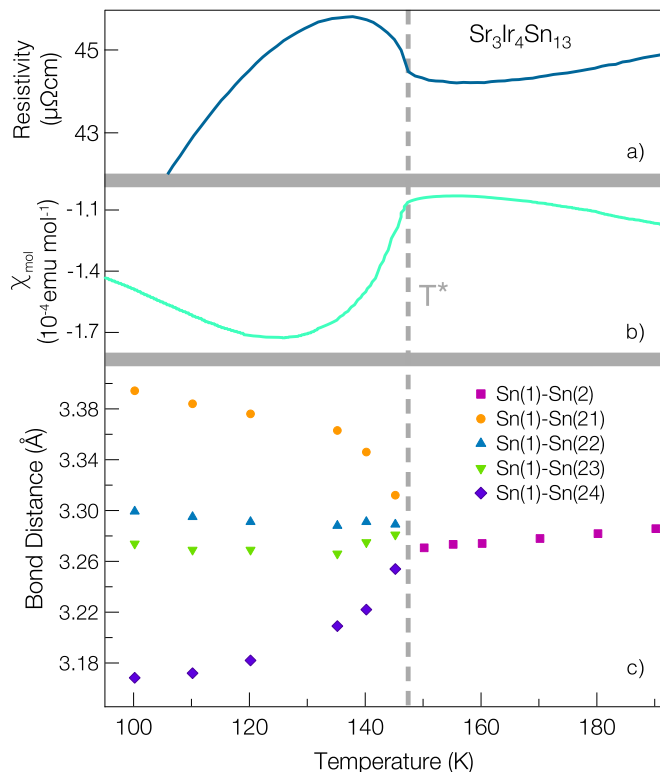


FIG. 1: Temperature dependence of (a) the electrical resistivity, (b) the magnetic susceptibility, and (c) interatomic bond-lengths. The bond-length between the Sn atom in the centre of the Sn_{12} cage, Sn(1), and the cage atoms, Sn(2), in the I -phase, splits into four distinct lengths in the I' -phase below $T^* \simeq 147$ K (dashed line). The symbol sizes represent the measurement accuracy. The observed anomalies near T^* are consistent with a superlattice transition.

of the high temperature phase ($R1$, $wR2$ and χ^2 of 4.4 %, 13.9 % and 1.1 %, respectively). The transformation into the I' -phase commences at the same temperature, T^* , where distinct anomalies are observed in the resistivity and the magnetic susceptibility (Fig. 1). Since these superlattice reflections are very faint – less than 1% of the parent lattice intensity – it is conceivable that similar superlattice transitions in other 3-4-13s have been overlooked.

Resistivity ρ measurements under hydrostatic pressure on $\text{Sr}_3\text{Ir}_4\text{Sn}_{13}$ show that T^* decreases rapidly with increasing pressure, whereas T_c rises slowly (Fig. 3). This pattern carries over to $\text{Ca}_3\text{Ir}_4\text{Sn}_{13}$ (Fig. 4), which due to its smaller unit cell volume can be regarded as a high pressure analogue of $\text{Sr}_3\text{Ir}_4\text{Sn}_{13}$. Here, T^* and the associated anomaly broadens and shifts towards lower temperature with increasing pressure, extrapolating to 0 K at a critical pressure of $p_c \simeq 18$ kbar. Near this critical pressure, $\rho(T)$ is linear over a wide temperature range, from T_c up to 50 K (Fig. 4). Anvil cell AC susceptibility measurements extend the available pressure range and show that T_c peaks near 8.9 K at ~ 40 kbar.

Analysis of the pressure dependence of T^* and T_c of intermediate substitution values x suggests that the chemical pressure effect of fully substituting Ca with Sr places $\text{Sr}_3\text{Ir}_4\text{Sn}_{13}$ at roughly -52 kbar relative to the physi-

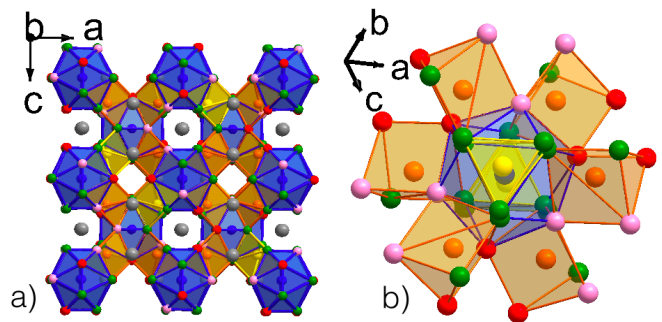


FIG. 2: (a) Overall view of the I' structure at 100 K and (b) the $\text{IrSn}(2)_6$ trigonal bipyramids around one $\text{Sn}(1)\text{Sn}(2)_{12}$ icosahedra. The Ir(1), Ir(2) and Sn(1) atoms, and their polyhedra, are orange, yellow and dark blue respectively, and the Sr atoms are grey. The Sn(2) type atoms with the shortest, medium and the longest bond distances to Sn(1) are light pink, green and red. In the high temperature I -phase, the bond distances in the $\text{IrSn}(2)_6$ trigonal prisms and $\text{Sn}(1)\text{Sn}(2)_{12}$ icosahedra are identical. In the I' -phase, however, a distortion of the Sn(1) icosahedra gives rise to four groups of three identical bond distances, namely Sn(1)-Sn(21-24) (see Fig. 1c). This distortion occurs in concert with tilting of three-quarters of the trigonal prisms while those whose axis are along the (111) direction, thereby containing Ir(2), remain untilted.

cal pressure scale of $\text{Ca}_3\text{Ir}_4\text{Sn}_{13}$. According to Vegard's law the lattice parameters of a substitution series are directly proportional to the substitution percentage; therefore, the intermediate values $x = 0.50$ and 0.75 can be placed at -26 and -13 kbar, respectively. This allows us to construct a universal temperature-pressure phase diagram for the entire $(\text{Ca}_x\text{Sr}_{1-x})_3\text{Ir}_4\text{Sn}_{13}$ series (Fig. 5).

The superconducting dome – which peaks close to where an ordered state is completely suppressed – and the anomalous quasi-linear $\rho(T)$ are reminiscent of quantum critical phenomena observed in correlated electron systems on the threshold of magnetism [18]. There is, however, no evidence that the $(\text{Sr}/\text{Ca})_3\text{Ir}_4\text{Sn}_{13}$ low temperature order is magnetic. On the contrary, the fact that no magnetic order has been reported in any I' -phase material without rare-earth constituents; the low absolute magnetic susceptibility values; the absence of clear anisotropy in the susceptibility at T^* ; the spin polarised band structure calculations within density functional theory for various hypothetical magnetic states, in which the magnetic moments collapse to zero in all cases; and the strong indications that the superconducting state is conventional and fully gapped [19] all point towards a non-magnetic transition at T^* .

An alternative explanation for the reported observations examines the interplay between a purely structural, non-magnetic superlattice formation and the electronic structure. In high electron density systems like $(\text{Sr}/\text{Ca})_3\text{Ir}_4\text{Sn}_{13}$, some electronic bands form Fermi surfaces which occupy large portions of the Brillouin zone. The period-doubling associated with the superlattice causes the Brillouin zone to shrink and consequently the Fermi surface to reconstruct, gapping out sections of the Fermi surface, thereby reducing the electronic density of

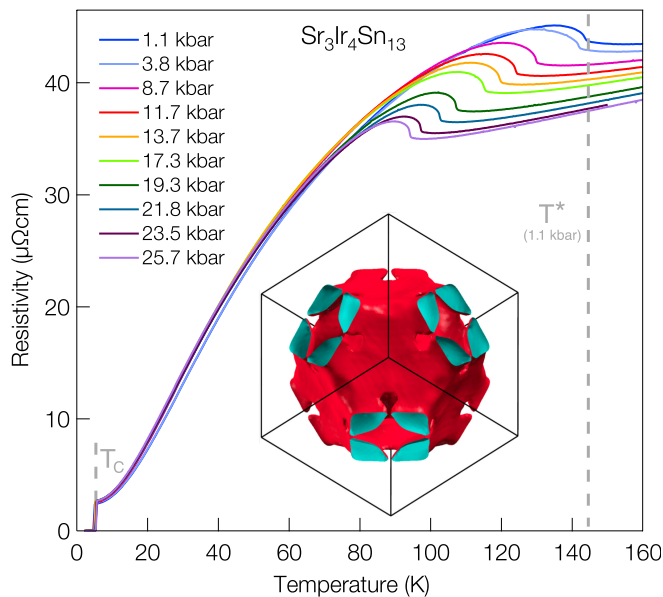


FIG. 3: The main panel shows the temperature dependence of the electrical resistivity, $\rho(T)$, in $\text{Sr}_3\text{Ir}_4\text{Sn}_{13}$ as a function of applied hydrostatic pressure, which allows the tracking of both the superlattice and the superconducting transitions. The inset shows the high temperature I -phase $\text{Sr}_3\text{Ir}_4\text{Sn}_{13}$ Fermi surface of band 329, where a large, flat region normal to the body-diagonal of the Brillouin zone can be seen.

states at the Fermi level. This can explain the rise in $\rho(T)$ and the drop in the magnetic (Pauli) susceptibility at T^* . When T^* is suppressed with hydrostatic pressure, the full high temperature density of states survives to low temperatures, which causes T_c to increase.

The linear $\rho(T)$ near p_c suggests that this simple argument, based solely on the electronic density of states near the Fermi level, does not fully capture the key observations. If the superlattice transition remains second order, or only weakly first order, then the minimum frequency Ω of the associated optical phonon mode should go soft at T^* , which itself approaches zero at p_c . The observed linear $\rho(T)$ could then be ascribed to scattering from this low-lying optical mode, which according to the equipartition theorem contributes to the variance of the atomic displacement in proportion to temperature when $k_B T > \hbar\Omega$.

This softening of parts of the phonon spectrum can help explain the shape of the superconducting dome. In the Eliashberg-McMillan treatment, T_c is sensitive to the electron-phonon coupling parameter $\lambda = N(E_F)\langle I^2 \rangle / M\langle \omega^2 \rangle$, where $N(E_F)$ is the density of states, $\langle I^2 \rangle$ the electron-phonon matrix element averaged over the Fermi surface, M the atomic mass and $\langle \omega^2 \rangle$ a weighted average of the square of the phonon frequency. The suppression of T^* reduces the partial gapping of the Fermi surface, enhancing $N(E_F)$, while softening of parts of the phonon spectrum reduces $\langle \omega^2 \rangle$. If all other parameters are constant, then T_c increases with increasing λ . Consequently, the enhancement of $N(E_F)$ with pressure, along with softening of phonon frequencies, give rise to an increase in T_c through the enhancement of λ .

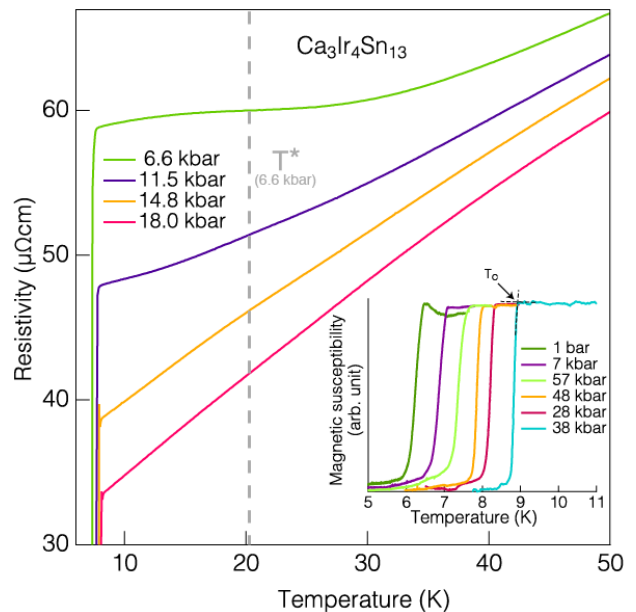


FIG. 4: (Main panel) Temperature dependence of the electrical resistivity, $\rho(T)$, in $\text{Ca}_3\text{Ir}_4\text{Sn}_{13}$ as a function of applied hydrostatic pressure. T^* is defined as the minimum of $d\rho/dT$, which broadens on approaching the critical point; this is why T^* is lower than the onset temperature. Near the critical pressure $p_c \simeq 18$ kbar, where T^* extrapolates to 0 K, $\rho(T)$ assumes a linear temperature dependence over a large temperature range. (Inset) Pressure dependence of the magnetic susceptibility in $\text{Ca}_3\text{Ir}_4\text{Sn}_{13}$. T_c peaks near 8.9 K at about 40 kbar and then decreases with further increasing pressure.

With further increase in pressure, the optical mode associated with the superlattice transition stiffens again, raising $\langle \omega^2 \rangle$ and suppressing T_c . More detailed theoretical calculations accounting for the effect of the energy scale prefactor in the McMillan formula will be required to describe the observed phase diagram quantitatively.

In order to investigate the origin of the superlattice transition we have carried out band structure calculations. In the I -phase, six bands cross the Fermi level. Each sheet of the Fermi surface is three dimensional, but some exhibit low curvature regions with the necessary characteristics for nesting: the flat sections of band 329 (Fig. 3 inset) are strong candidates. The contribution of this band to the computed unrenormalised, wavevector-dependent charge susceptibility $\chi(\mathbf{q})$, or Lindhard function, peaks at $\mathbf{q} = (1/2, 1/2, 1/2)$, with a 21% enhancement above that at the Brillouin zone centre, which is consistent with the transition to the I' -phase. This confirms the visual impression that sections of the Fermi surface nest along the body diagonal, and suggests that the superlattice transition is indeed connected to a charge density wave (CDW) instability of the conduction electron system.

Investigations into the effect of lattice instabilities on superconductivity have a long history, starting with the structurally related A15 compounds [20, 21]. Examples of CDW-driven lattice instabilities include $\text{Lu}_5\text{Ir}_4\text{Si}_{10}$ [22], dichalcogenides such as TiSe_2 [23] and TaS_2 [24], intercalated graphite CaC_6 [25] and 1- or 2-D organic com-

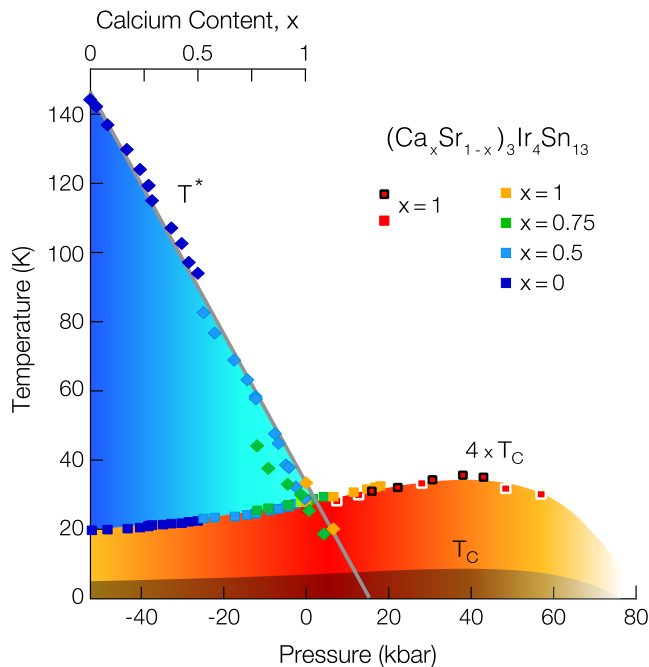


FIG. 5: By placing $x = 0, 0.50$ and 0.75 at $-52, -26$ and -13 kbar, respectively (c.f. top axis), a universal phase diagram can be constructed for $(\text{Ca}_x\text{Sr}_{1-x})_3\text{Ir}_4\text{Sn}_{13}$. The superlattice transition temperature, T^* , extrapolates to zero temperature at roughly 18 kbar, giving rise to a structural quantum critical point. The red ($x = 1$) symbols denote values derived from AC susceptibility measurements – the white (black) borders represent a pressure medium of glycerin (4:1 methanol:ethanol). The remaining data are obtained from the analysis of resistivity measurements. The superconducting transition temperature, T_c , is multiplied by 4 for clarity.

pounds [26, 27]. There is an emerging view that in most cases the evolution of the phonon spectrum with tuning parameters like pressure crucially influences T_c , both by boosting it when the lattice instability is suppressed, and by reducing it again when pressure is increased further [28]. Whereas most of the aforementioned materials are low-dimensional, very few clear cases of CDW order in 3D materials exist, notably CuV_2S_4 [29], which is not superconducting, and $\alpha\text{-U}$ [30], which has a lower symmetry structure. $(\text{Sr}/\text{Ca})_3\text{Ir}_4\text{Sn}_{13}$ allows us to investigate the interaction between a structural instability and superconductivity in a cubic material. Our study clarifies the nature of the previously unidentified phase transition in $(\text{Sr}/\text{Ca})_3\text{Ir}_4\text{Sn}_{13}$, which we interpret as an electronically driven superlattice distortion; it demonstrates that this transition can be tuned to zero temperature, leading to a structural quantum critical point; and it attributes the linear $\rho(T)$ and the dome structure of T_c to the softening of optical phonon modes around the structural quantum critical point. The prospect of fine-tuning phonon frequencies by controlling a structural transition temperature, and the precise control over the lattice structure exemplified in this study, motivate further studies in this material class as well as in more complex systems, where spin and charge density wave transitions may be correlated.

Acknowledgement. We particularly thank G. G. Lonzarich, C. Pickard, and D. Khmelnskii for helpful discussions. This work was supported by the EPSRC UK, Trinity College (Cambridge), Grant-in-Aid for Scientific Research from the JSPS (22350029), Global COE Program “International Center for Integrated Research and Advanced Education in Materials Science”, Kyoto University, from the MEXT Japan. SKG acknowledges the Great Britain Sasakawa Foundation for travel grant and Kyoto university for hospitality.

* Electronic address: skg27@cam.ac.uk

† Current address: Department of Chemistry, University of Bath, Bath BA2 7AY, United Kingdom

- [1] I. BERSUKER, *The Jahn-Teller Effect*, Cambridge University Press (2006).
- [2] P. A. LEE, T. M. RICE, and P. W. ANDERSON, *Phys. Rev. Lett.* **31**, 462 (1973).
- [3] J. REMEIKA, G. ESPINOSA, A. COOPER, H. BARZ, J. ROWELL, D. MCWHAN, J. VANDENBERG, D. MONCTON, Z. FISK, L. WOOLF, H. HAMAKER, M. MAPLE, G. SHIRANE, and W. THOMLINSON, *Solid State Communications* **34**, 923 (1980).
- [4] G. P. ESPINOSA, *Mater. Res. Bull.* **15**, 791 (1980).
- [5] H. SATO, T. FUKUHARA, S. IWAKAWA, Y. AOKI, I. SAKAMOTO, S. TAKAYANAGI, and N. WADA, *Physica B* **186-88**, 630 (1993).
- [6] A. M. STRYDOM, *J. Phys.:Condens. Matter* **19**, 386205 (2007).
- [7] J. HODEAU, M. MAREZIO, J. REMEIKA, and C. CHEN, *Solid State Communications* **42**, 97 (1982).
- [8] S. MIRAGLIA, J. HODEAU, M. MAREZIO, C. LAVIRON, M. GHEDIRA, and G. ESPINOSA, *J. Solid State Chem.* **63**, 358 (1986).
- [9] P. BORDET, D. COX, G. ESPINOSA, J. HODEAU, and M. MAREZIO, *Solid State Communications* **78**, 359 (1991).
- [10] J. YANG, B. CHEN, C. MICHIOKA, and K. YOSHIMURA, *J. Phys. Soc. Jpn.* **79**, 113705 (2010).
- [11] S. K. GOH, P. L. ALIREZA, P. D. A. MANN, A. M. CURNBERLIDGE, C. BERGEMANN, M. SUTHERLAND, and Y. MAENO, *Curr. Appl. Phys.* **8**, 304 (2008).
- [12] P. L. ALIREZA and S. R. JULIAN, *Rev. Sci. Instrum.* **74**, 4728 (2003).
- [13] L. E. KLINTBERG, S. K. GOH, S. KASAHARA, Y. NAKAI, K. ISHIDA, M. SUTHERLAND, T. SHIBAUCHI, Y. MATSUDA, and T. TERASHIMA, *J. Phys. Soc. Jpn.* **79**, 123706 (2010).
- [14] G. M. SHELDRIK, *Acta Crystallographica Section A* **64**, 112 (2008).
- [15] L. J. FARRUGIA, *J. Appl. Cryst.* **32**, 837 (1999).
- [16] J. P. PERDEW, K. BURKE, and M. ERNZERHOF, *Phys. Rev. Lett.* **77**, 3865 (1996).
- [17] K. SCHWARZ and P. BLAHA, *Computational Materials Science* **28**, 259 (2003).
- [18] N. D. MATHUR, F. M. GROSCHKE, S. R. JULIAN, I. R. WALKER, D. M. FREYE, R. K. W. HASSELWIMMER, and G. G. LONZARICH, *Nature* **394**, 39 (1998).
- [19] N. KASE, H. HAYAMIZU, and J. AKIMITSU, *Phys. Rev. B* **83**, 184509 (2011).
- [20] L. TESTARDI, *Rev. Mod. Phys.* **47**, 637 (1975).
- [21] S. TANAKA, A. MIYAKE, B. SALCE, D. BRAITHWAITE, T. KAGAYAMA, and K. SHIMIZU, *J. Phys.: Conf. Ser.* **200**, 012202 (2010).

- [22] R. SHELTON, L. HAUSERMANNBERG, P. KLAVINS, H. YANG, M. ANDERSON, and C. SWENSON, *Phys. Rev. B* **34**, 4590 (1986).
- [23] A. F. KUSMARTSEVA, B. SIPOS, H. BERGER, L. FORRO, and E. TUTIS, *Phys. Rev. Lett.* **103**, 236401 (2009).
- [24] B. SIPOS, A. KUSMARTSEVA, A. AKRAP, L. F. H. BERGER, and E. TUTIS, *Nature Materials* **7**, 960 (2008).
- [25] A. GAUZZI, S. TAKASHIMA, N. TAKESHITA, C. TERAKURA, H. TAKAGI, N. EMERY, C. HEROLD, P. LA-GRANGE, and G. LOUPIAS, *Phys. Rev. Lett.* **98**, 067002 (2007).
- [26] W. LUBCZYNSKI, S. V. DEMISHEV, J. SINGLETON, J. M. CAULFIELD, L. DU CROO DE JONGH, C. J. KEPERT, S. J. BLUNDELL, W. HAYES, M. KURMOO, and P. DAY, *J. Phys.: Condens. Matter* **8**, 6005 (1996).
- [27] J. WOSNITZA, *Curr. Opin. Solid State Mater. Sci.* **5**, 131 (2001).
- [28] M. CALANDRA and F. MAURI, *Phys. Rev. Lett.* **106**, 196406 (2011).
- [29] R. FLEMING, F. DISALVO, R. CAVA, and J. WASZCZAK, *Phys. Rev. B* **24**, 2850 (1981).
- [30] S. RAYMOND, J. BOUCHET, G. LANDER, M. L. TACON, G. GARBARINO, M. HOESCH, J.-P. RUEFF, M. KRISCH, J. LASHLEY, R. SCHULZE, and R. ALBERS, *Phys. Rev. Lett.* **107**, 136401 (2011).